Journal of *Marine Science and Engineering*

MDPI

Article

Modelling and Simulation Hydrodynamics Processes in Liquefied Natural Gas Transportation Systems

Marijonas Bogdevicius [1], Vigaile Semaskaite [1], Tatjana Paulauskiene [2,*], Jochen Uebe [2] and Algimantas Danilevicius [1]

[1] Department of Mobile Machinery and Railway Transport, Faculty of Transport Engineering, Vilnius Gediminas Technical University, Plytines St. 27, 10105 Vilnius, Lithuania
[2] Engineering Department, Faculty of Marine Technology and Natural Sciences, Klaipeda University, H. Manto 84, 92294 Klaipeda, Lithuania
* Correspondence: tatjana.paulauskiene@ku.lt

Abstract: Global natural gas resources are growing and are increasingly geographically diverse. A Floating Storage and Regasification Unit (FSRU) is one of the most commonly used vessel types in the global ship fleet due to the possibility of storage, reloading to another ship, and regasifying it for re-injection into the natural gas grid. It is important to control system parameters for reliable technological processes such as tank hydrostatic pressure, vapor pressure, LNG density, LNG temperature, and phase changes between liquid and gas states. Additionally, pressure monitoring is important to control during transit in port and bunkering to prevent the pressure in the tanks from exceeding the tank design pressure. In this research study, a comprehensive hydrodynamic model for an LNG storage tank in a real-life regasification terminal (Floating Storage and Regasification Unit, LNG Terminal of Klaipeda City, Lithuania), operating in transportation mode to the regasification unit, was created. For this research, LNG is investigated as a compressible liquid and the speed of sound in LNG is evaluated. A complex mathematical model of the system allows the analysis of high-speed hydrodynamic and dynamic processes at cryogenic temperature (110 K) and evaluates the geometric parameters (tank geometry, electric motors and pumps, pipe geometric parameters, and roughness of internal surfaces) and the characteristics of pumps and electric motors. The complex mathematical model of the system was implemented using Fortran programing language and MATLAB R28a. It determined the parameters (pressure, velocity, liquid level of LNG in the tanks, electric motor angular velocity, torques, hydraulic energy losses, etc.) of the system during its start-up mode (until 5 s). It was found that hydraulic energy losses in all pipes contain 1.7% of the whole system power (the total power of the electric motors is 3132 kW). In case of increasing energy costs, this model could be used to control energy losses during the operation of the FSRU in various technological modes.

Keywords: liquefied natural gas; maritime infrastructure; liquefied natural gas transportation system; floating storage and regasification unit; method of characteristics; modelling

Citation: Bogdevicius, M.; Semaskaite, V.; Paulauskiene, T.; Uebe, J.; Danilevicius, A. Modelling and Simulation Hydrodynamics Processes in Liquefied Natural Gas Transportation Systems. *J. Mar. Sci. Eng.* **2022**, *10*, 1960. https://doi.org/10.3390/jmse10121960

Academic Editor: Md Jahir Rizvi

Received: 8 November 2022
Accepted: 7 December 2022
Published: 9 December 2022

1. Introduction

As highlighted in the European Green Deal, transport accounts for a quarter of the European Union's (EU) greenhouse gas emissions, and this figure is still growing. To achieve climate neutrality in the sense of the Paris Climate Agreement, current transport emissions would have to be reduced by 90% by 2050 [1].

The use of alternative fuels, such as Liquid Natural Gas (LNG), could contribute to reducing greenhouse gas emissions. As outlined in DNV GL's Technology Outlook 2025 [2], global demand for gas as an environmentally friendly alternative to conventional marine fuels has more than doubled in the past 30 years and it will continue to increase [3].

Global natural gas resources are growing, and their geographic diversity is increasing [4]. The LNG shipping industry kept pace with this growth, adding 57 carriers and

4 Floating Storage and Regasification Units (FSRUs) to a total of 641 active vessels by the end of April 2022, including patrol vessels, car ferries, cruise vessels, bulk carriers, container vessels and other types of LNG vessels [3,5]. The active fleet includes 45 FSRUs and 5 Floating Storage Units (FSUs), demonstrating the continued interest in flexible solutions to enable markets to start importing LNG or increase their LNG imports as energy demand grows. This illustrates shipowners' expectations that the LNG trade will continue to grow in line with the increase in liquefaction capacities in the coming years.

For markets to grow, LNG and electricity supply infrastructures and their services need to be open, transparent, and interoperable. By 2025, the EU should have completed the backbone of refueling infrastructure (up to EUR 945 million in the Trans-European Transport Network (TEN-T) Core Network Corridor seaports by 2025), providing full coverage of the TEN-T core network corridors [6]. Users also need to be able to use the whole transport network in a smooth and easy way—that is why synergies with other modes of transport should be examined as well.

LNG is natural gas converted into a liquid form. Condensation occurs at −162 °C, reducing its volume by 600 times (in comparison to the gaseous state), which makes LNG cost-efficient to transport over long distances.

Natural gas consists mainly of methane and compared to other fuels has very low amounts of sulphur oxides, nitrogen oxygens, and particulate matter when combusted [7]. LNG therefore not only easily complies with the sulphur emission caps but also meets the requirements for upcoming regulations on NOx reduction.

In addition, LNG produces less than 10% particulate matter and 50% fewer greenhouse gases than coal when used to generate electricity, 21% less than fuel oil in transportation, and has over 95% efficiency when used to heat homes [8]. In addition, according to DNV GL, ships powered by LNG can reduce CO_2 emissions by 15% to 20%.

Floating Storage and Regasification Units (FSRUs) are one of the most commonly used vessel types in the global ship fleet due to the possibility of storage, reloading to another ship, and regasifying it for re-injection into the natural gas grid. Commonly, an FRSU consists of special isolated tanks for LNG storage and handling inside the ship, and on the deck, there is regasification equipment, which converts LNG into a gaseous state for end users [9,10]. Observing LNG technological processes in FSRUs, the main focus is on LNG unloading, loading, and regasification modes [10]. So, it is important to control system parameters for reliable technological processes, such as hydrostatic pressure in the tanks, vapor pressure, LNG density, LNG temperature, and phase changes between liquid and gas states. Furthermore, pressure monitoring is important to control during transit in port and bunkering to prevent the pressure in the tanks from exceeding the tank design pressure. During loading and unloading modes, a detailed calculation for the maximum allowable LNG level in the filling tanks should be provided to prevent overfilling [11]. One of the main challenging processes of FSRUs is regasification. For the regasification process, low pressure (8–10 bar is commonly when the selected pump starts) and high-pressure pumps (80–120 bar) are used. At first, LNG is pumped by a low-pressure pump from the storage tank to the buffer tank or the recondenser unit. From there, the LNG is pumped by high pressure to the vaporizer.

Another challenge is the many pipes and pipelines of the LNG regasification pipeline system. One of the main tasks for engineers is to design a cryogenic pipeline with minimum length, ensuring the minimum energy losses related to the heating of liquid by heat input and hydraulic losses [12]. It is important to protect the work of the system from technical problems by technical maintenance of regasification equipment, including observation of technological parameters in pipelines. One of the solutions could be the LNG flow observation model in the regasification system.

Most mathematical models are described for natural gas flow in the pipelines. Generally, the flow of natural gas through high-pressure pipelines is governed by the partial differential equation (PDE) of mass and momentum conservation in conjunction with the equation of state (EOS) and is used with different methods to solve [13]. Only several

studies have been conducted for modeling LNG technological processes in pipelines, and more have been performed for LNG regasification equipment, for example in [14–17]. The authors of study [18] created a model based on thermal and hydraulic calculations of an underground cryogenic pipeline. This model allowed estimating the main production parameters such as pressure drop and temperature of LNG during its flow through the pipeline underground. In addition, this model permits calculations without initial parameters such as inlet pressure and diameter. One of the most important conditions is that the temperature should be below the boiling point of LNG at the given pressure, and the operating pressure should exceed the saturation pressure of LNG by at least 0.5 MPa. Another analytical model for describing the LNG flow in the pipeline was described in [19], which allows the determination of parameters such as pressure, temperature, density, and viscosity for a given composition as a function of pipeline length.

This paper presents the mathematical model for a real LNG transportation system at cryogenic temperature (110 K) starting from LNG pumping from the LNG tank to the Suction Drum and pumping to the LNG vaporizer of the regasification unit. These processes are the most important for reliable further regasification equipment work. The model investigates hydrodynamic and dynamic high-velocity processes in the unsteady fluid flow when the LNG is transferred to the regasification unit and allows observing pressure changes, LNG velocity and the speed of sound in the LNG at the piping points in the system during system start-up (until 5 s). The universality of this model is that there are a lot of variables in the system to determine and it allows for evaluation by the different technologic parameters of changing lengths and diameters of pipes, liquid level, volume in the tanks, and electric motors parameters, or it uses another fluid in cases when fluid parameters are known. Of special interest to this model is that characteristics, pressure losses, and hydrodynamic processes of multistage centrifugal pumps are verified when operating in different technological regimes when LNG flow enters the LNG regasification unit. Furthermore, the work of the electric motor of the transportation pump of the main LNG tank is a part of the dynamic process observation in this model. The model is validated using technical data that characterize real technological regimes of regasification in the Floating Storage and Regasification Unit.

2. Research Methodology

2.1. Symbols and Notations

Table 1 shows the symbols used in this work.

Table 1. Symbols and Notations.

Symbol	Meaning
L1, L2, L3, L4, L5, L6, L7, L8	the different section of pipes in the LNG transportation system
EM1, EM2, EM3, EM4	electric motor indexes of pumps
pv1	vapor pressure of BOG in the LNG tank, Pa
pv2	vapor pressure of BOG in the Suction Drum, Pa
TI1	LNG temperature in the LNG tank, K
TI2	LNG temperature in the Suction Drum, K
$H_{tank1}(t)$	liquid level in the tank by the time changing in the LNG tank, m
$H_{tank1,0}$	height between the pump and the bottom of the LNG tank, m
$H_{tank2}(t)$	liquid level in the tank by the time changing in the Suction Drum, m
g	gravitational acceleration, m/s
A_1 and A_2	cross-sectional areas of the LNG liquid surface in the LNG tank and in the Suction Drum, m^2
$Q_{1,in}$ and $Q_{L1,out}$	LNG volume flow of the pipeline (L1) inlet and outlet, m^3/s
$Q_{2,in}$	LNG volume flow of the pipeline (L2) inlet, m^3/s

Table 1. *Cont.*

Symbol	Meaning
ρ_l	LNG density, kg/m^3
M_{mix}	molecular mass of mixture, kg/kmol
x_i	molar fraction of constituent i
V_{mix}	molar volume of component i at the temperature of LNG, m^3
V_i	molar volume of constituent i at the temperature of LNG, m^3
x_i	molar fraction of constituent i, mol
k_1, k_2	volume correction factors, mol/l
$T_{c,i}$	critical temperature of constituent i, K
c_{EM1}, d_{EM1}	parameters of the electric motor
ω_{EM1}	angular velocity of the electric motor, rad/s
I_{EM1}	mass inertia moment of the rotor of electric motor and pump's rotor
c_1	damping coefficient
$M_{pump1}\left(\omega_{EM1}, p_{pump1}\right)$	load torque of the electric motor's rotor
Q_{pump1}	total flow of Submerged Motor Pump (SMR) pump, m^3/s
η_{pump1}	coefficient of SMR pump
$p_{pump1}\left(Q_{pump1,}\omega_{EM1}\right)$	total SMR pump characteristic
$Q_{L1,1}$	LNG flow in the first section of pipeline, m^3/s
$p(Q_{pump1,0})$	total SMR characteristic at an angular velocity $\omega_{EM1,0}$
$A_{p,in}$	sec tion area between point N and V_{p1}, m^2
$L_{p,in}$	length between point N and $p_{p,1}$, m
p_N	pressure of inlet pipe, Pa
$p_{p,1}$	pressure of the passage between the pipe and the first stage of pump's joint, Pa
$\Delta p_{p,in}$	pressure losses between point N and p_{p1}, Pa
sign$\left(G_{p,in}\right)$ and sign$\left(G_{p,out}\right)$	sign function, which indicates LNG mass flow direction
$K\left(p_{p,1}\right)$	bulk modulus of elasticity of LNG, Pa
G_{p12}	LNG mass flow between $p_{p,1}$ and $p_{p,2}$, kg/s
$\rho_l\left(p_N\right)$	LNG density in inlet pipe, kg/m^3
$\rho_l\left(p_{p,1}\right)$	LNG density in the passage between the pipe and the first stage of pump's joint, kg/m^3
$K\left(p_{p,2}\right)$	bulk modulus of elasticity of LNG, Pa
G_{p12}	LNG mass flow between $p_{p,1}$ and $p_{p,2}$, kg/s
$\rho_l\left(p_{p,1}\right)$ and $\rho_l\left(p_{p,2}\right)$	LNG density of $Vp_{,1}$ and $Vp_{,2}$, kg/m^3
$G_{p,out}$	mass flow of LNG from outlet of pump to the outlet pipe, kg/s
$A_{p,in}$	sec tional area between p_{p2} and point 1, m^2
$L_{p,in}$	length between p_{p2} and point 1, m
p_{p1}	pressure of the passage between the pipe and the first stage of pump's joint, Pa
p_{p2}	pressure of the passage between the first stage of pump's joint and the outlet pipe, Pa
Δp_{pout}	pressure losses between p_{p2} and point 1, Pa

Table 1. *Cont.*

Symbol	Meaning
ρ_l	density of LNG, kg/m^3
υ	velocity of LNG, m/s
$A(x)$	cross-sectional area of a pipeline, m^2
p	LNG pressure, Pa
$\Pi(x)$	the perimeter of cross-section of the pipeline, m
τ	tangential fluid stress on the inner surface of the pipeline, Pa
a_x	the acceleration along the x axis, m^2/s
α	angle between horizontal axis and center line of pipe
c	speed of sound in the LNG, m/s
$K(p,T)$	bulk modulus of elasticity of liquid, Pa
E	modulus of elasticity of a pipeline, Pa
D_{in}	internal diameter of a pipeline, m
e	thickness of a wall of a pipeline, m
$[J]_{i-1}$	Jacobi matrix
$\{\Delta Y\}_i$	increment vector of unknown variables
i	number of iterations
C_r	Courant number
$Q_{L2,N}$, $Q_{L3,1}$, $Q_{L4,1}$, $Q_{L5,1}$, Q_{Losses}	LNG volume flow, m^3/s
$Q_{Losses}(p_{V3})$	losses of LNG volume flow, m^3/s
$p_{Lk,0}$	constant pressure in the pipes
A_{Lk}	cross-section area of pipe k, m^2
$A_{channel,k}$	cross-section area of channel of k-th BOG recondenser, m^2
$n_{channel,k}$	number of channels of k-th BOG recondenser

2.2. Description of LNG Transportation System

The basic components of the LNG transportation system in the FSRU are presented in Figure 1. The technological process starts when a submerged cargo pump from the LNG Tank transports the LNG at high pressure to a vapor-liquid separator (Suction Drum) on deck. The pipeline system from the LNG tank to the Suction Drum is divided into different sections of diameters. Different diameters of pipelines are used to minimize pressure losses in the system, in that case decreasing LNG flow in separate sections. All the pipelines of the system are marked with the letter L with a number, which is essential for calculation in further mathematical modeling.

When LNG has been transported to the Suction Drum, the LNG starts mixing with the Boil of Gas (BOG). The Suction Drum has two functions to maintain constant LNG pressure, which is required to operate the compression pumps (High-Pressure Booster Pumps), and to condensate BOG from the LNG tanks. In this research, BOG mixing between LNG is not analyzed and so BOG is not marked in the simplified scheme. From the Suction Drum, the LNG is transported to the regasification equipment by a high-pressure intensifier pump. Usually, there are several regasification trains, one of which serves as a reserve. In this model, three parallel regasification trains are considered as an example (a train is a typical regasification line consisting of the same regasification equipment as the high-pressure booster pump, the BOG recondenser, the LNG vaporizer, etc.). Firstly, LNG flow goes to the Pipeline Unit to separate LNG flow, and then it is divided into three LNG flows, which are connected to regasification lines. Three regasification lines (regasification lines indicated as

L3, L4, and L5) are always in working modes. After introducing the LNG transportation system, the mathematical model of the LNG transportation system including descriptions of LNG equipment is presented in the following sections.

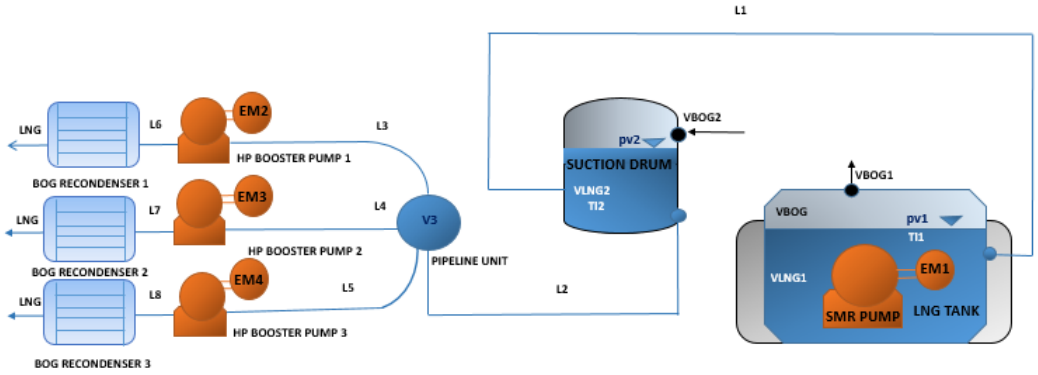

Figure 1. Simplified scheme of LNG transportation system in the FSRU. Note: L1, L2, L3, L4, L5, L6, L7, L8 is presented to illustrate the different section of pipes in LNG transportation system; EM1, EM2, EM3, EM4—electric motor indexes of pumps; pv1—vapor pressure in the LNG tank; pv2—vapor pressure in the Suction Drum; TI1—LNG temperature in the LNG tank; TI2—LNG temperature in the Suction Drum.

2.3. Model Assumptions and Evaluations

As previously described, the LNG transportation system, which is operating in different technological regimes, and a full mathematical model are built, involving individual mathematical models of equipment for technological parameter observation (Sections 2.4–2.6). For the whole system mathematical model, LNG flow in pipes is connected to system devices (tanks and pumps) using boundary conditions (Section 2.7). The main goal of this complex model is that by changing one of the technological parameters, it allows us to observe the impact to the whole system. The principal scheme of the mathematical model of the total system is introduced below in Figure 2.

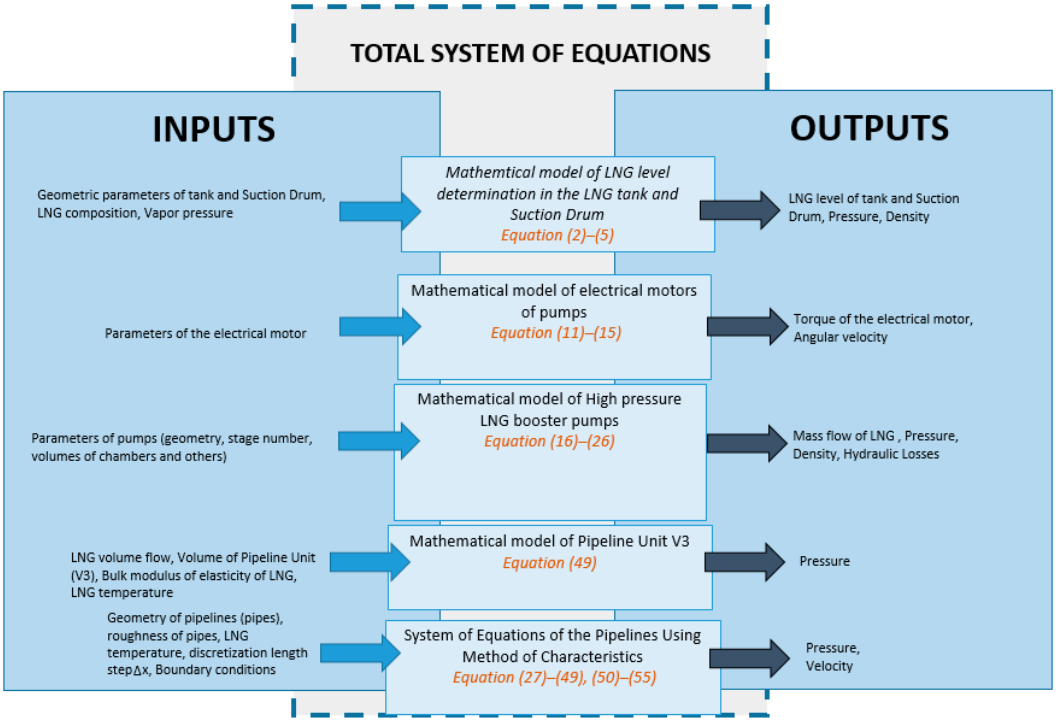

Figure 2. Principal scheme of the mathematical model.

The key assumptions used for mathematical models are as follows:

- The LNG tank and the Suction Drum vapor pressures (pv1 and pv2) are assumed to be constant. From other scientific studies, it was verified that the vapor pressure changes slowly. In real systems, it changes during the day or week, etc. In our model, it is important to observe the parameters of the system when the LNG transportation system starts working to verify that the model works properly at the beginning. The solution time of the model is chosen to be 5 s, so the vapor pressures do not change drastically at this time.
- LNG temperatures (Tl1 and Tl2) are assumed to be constant due to the small heat transfer between walls and LNG in the LNG tank and the Suction Drum. For this reason, the system must be fully insulated, and the heat transfer between walls and LNG in the LNG tank and the Suction Drum is therefore very low. Otherwise, the system will not work because LNG will start evaporating and will not characterize real-life regasification cases in the FSRU.
- The height of the liquid level of LNG in the tank (Htank1(t)) and the Suction Drum (Htank2(t)) varies in the LNG transportation system. The height of the liquid level of LNG in the tank strongly affects hydrodynamic processes in the system, especially in the pipeline L1, when LNG starts transferring from one tank (LNG tank) to another (Suction Drum). Additionally, the height of the liquid level is a good indicator of start-process and end time.
- LNG composition is assumed to be 91.798 mol% methane, 5.698 mol% ethane, 1.303 mol% propane, 0.396 mol% n-butane and 0.805 mol% nitrogen. The composition has an impact on BOG generation, density changes, and evaporation rate. So, the composition was selected from real-life regasification cases in FSRUs (LNG Terminal of Klaipeda City, Lithuania), which is important for end users.

2.4. Description and Mathematical Model of LNG Tank and Suction Drum

The model configuration starts with hydrodynamics processes such as LNG level observations in the LNG tank (Htank1(t)) and the Suction Drum (Htank2(t)) when the first pump (the submerged motor cargo pump) starts working. The FSRU of this model shall include double-insulated tanks with inner shells. The containment system functions are to contain LNG cargo at approximately a temperature of −163 °C and insulate the cargo from the hull structure. The simplified scheme of one of the LNG tanks is introduced in Figure 3. Transportation of LNG from the LNG tank to the Suction Drum is part of the regasification process. The Suction Drum is a vertical vessel to balance pressure for further regasification steps. Additionally, the Suction Drum operates as a buffer tank for the following Higher-Pressure Booster Pumps, ensuring that there is always sufficient LNG available to the pumps when the pumps are operating at maximum capacity. The liquid-level observation is shown in Figures 3 and 4.

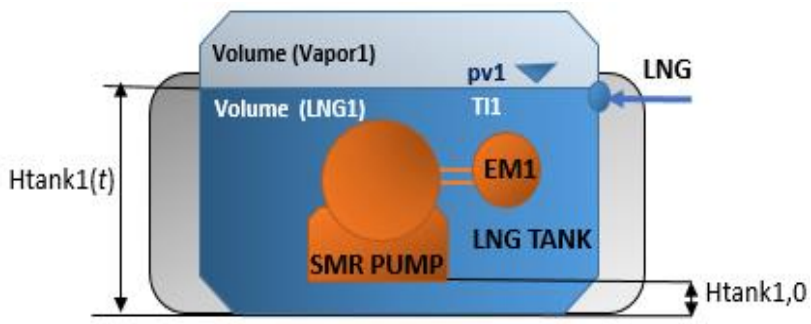

Figure 3. LNG level observation in the LNG tank.

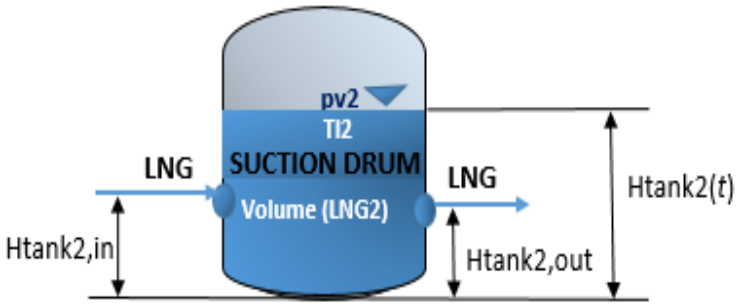

Figure 4. LNG level observation in the Suction Drum.

Hence, the operation of the LNG tank and the pump is described by the system of differential equations for estimating the pressure and the LNG level change in the LNG tank and the Suction Drum, according to Equations (2) and (5):

(a) The LNG tank:

$$p_{1,in} = (H_{tank1}(t) - H_{1,0}) \cdot \rho_l \cdot g + pv1 \quad (1)$$

Level of LNG in the tank:

$$\dot{H}_{tank1}(t) = -\frac{A_1}{A_{tank1}} Q_{1,in} \quad (2)$$

(b) The Suction Drum

$$p_{2,in} = (H_{tank2}(t) - H_{tank2,in}) \cdot \rho_l \cdot g + pv2 \quad (3)$$

$$p_{2,out} = (H_{tank2}(t) - H_{tank2,out}) \cdot \rho_l \cdot g + pv2 \quad (4)$$

Level of LNG in the Suction Drum:

$$\dot{H}_{tank2} = \frac{1}{A_{tank2}} [Q_{2,in} - Q_{L1,out}] \quad (5)$$

where: $H_{tan\,k1}(t)$—liquid level in the tank by the time changing in the LNG tank, m; $H_{tan\,k1,0}$—height between the pump and the bottom of the LNG tank, m; pv1 and pv2—vapor pressure of BOG in the LNG tank and the Suction Drum, Pa; g—gravitational acceleration, m/s; A_1 and A_2—cross- sectional areas of the LNG liquid surface in the LNG tank and in the Suction Drum, m^2; $A_{tan\,k1}$ and $A_{tan\,k2}$—cross-section areas of the LNG tank and the Suction Drum, m^2; $Q_{1,in}$ and $Q_{L1,out}$—LNG volume flow of the pipeline (L1) inlet and outlet, m^3/s; $Q_{2,in}$ — LNG volume flow of the pipeline (L2) inlet, m^3/s; ρ_l—LNG density, kg/m^3, determined according to the Enhanced Revised Klosek–McKinley method (ERKM) method by Equation (6). Commonly, this method is popular in the gas industry and is used under cryogenic conditions [20–22]. Additionally, the ERKM method is valid under pressures up to 10 MPa and the temperature varies from 115 K to 135 K [23].

$$\rho_l = \frac{M_{mix}}{V_{mix}} \cdot \left[1 + 406 \cdot \left(p_l - p_{s,corr}\right) \cdot \left(\frac{T_{pc}}{T_{pc} - T}\right)^{1,77}\right] \quad (6)$$

where: 406—constant and it is converted from MPa to Pa [23].

Molecular mass of the mixture is expressed by following equation:

$$M_{mix} = \sum M_i \cdot x_i \quad (7)$$

where: M_{mix}—molecular mass of mixture, kg/kmol; x_i—molar fraction of constituent i.

$$V_{mix} = \sum M_i \cdot V_i - \left[K_1 + (k_2 - k_1) \cdot \left(\frac{x_{N_2}}{0.0425}\right)\right] \cdot x_{CH_4} \quad (8)$$

where: V_{mix}—molar volume of component i at the temperature of LNG, m^3; V_i—molar volume of constituent i at the temperature of LNG, m^3; x_i—molar fraction of constituent i, mol; k_1, k_2—volume correction factors, mol/l; 0.0425—constant for the LNG with the content of nitrogen or butane content less than 4% [20,24].

Pressure correction for partial pressure (saturation) is described Equation (9):

$$p_{s,corr} = p_{s,CH4} + x_{N2} \cdot 0.11\ \text{MPa} \cdot (T - 90\ \text{K}) - x_{C2H6} \cdot 0.05\ \text{MPa} \cdot (T - 95\ \text{K}) \quad (9)$$

where: 0.11 MPa and 0.05 MPa are determined according to [23].

Pseudo critical temperature:

$$T_{pc} = \sum_i x_i \cdot T_{c,i} \quad (10)$$

where: x_i—molar fraction of constituent, mol; $T_{c,i}$—critical temperature of constituent i, K.

2.5. Description and Characteristics of LNG Submerged Cargo Pump and Electric Motor

To analyze the dynamic process of the LNG transportation system, the model is performed separately for the electric motor (EM1) of the transportation pump in the LNG tank. The submerged motor cargo pump (SMR) operates in the system of this model as in the real-case operation of the FSRU. The submerged motor cargo pump [25] casing and outer frame of the motor are combined with a flange joint as one unit. One of the main advantages of this type of pump is that it can shift from maximum flow to minimum flow smoothly following a stable head/capacity curve, even when shutting down, to ensure stable operation without noise and vibration [26]. The pump has a submerged motor with windings, which is cooled by the pumped LNG. So, LNG is used to lubricate and cool the pump and the motor bearings [27]. The SMR-type pump could reach the maximum flow of 520 m^3/h, which can be reduced to 220 m^3/h according to clients' LNG regasification demands.

At the beginning of the work of the SMR pump, the torque of the electric motors is described by the differential equation [28]:

$$\dot{M}_{EM1} = c_{EM1}(\omega_{EM10} - \omega_{EM1}) - d_{EM1} M_{EM1} \quad (11)$$

where c_{EM1}, d_{EM1}—parameters of the electric motor; ω_{EM1}—angular velocity of the electric motor, rad/s.

Equation of rotation of the electric motor's rotor in the SMR is equal to:

$$I_{EM1} \dot{\omega}_{EM1} = M_{EM1} - M_{pump1}\left(\omega_{EM1}, p_{pump1}\right) - c_1 \omega_{EM1} \quad (12)$$

where I_{EM1}—mass inertia moment of the rotor of electric motor and pump's rotor; c_1—damping coefficient; $M_{pump1}\left(\omega_{EM1}, p_{pump1}\right)$—load torque of the electric motor's rotor.

$$M_{pump1}\left(\omega_{EM1}, p_{pump1}\right) = \frac{p_{pump1}\left(Q_{pump1}, \omega_{EM1}\right) Q_{L1,1}}{\eta_{pump1} \omega_{EM1}} \quad (13)$$

where Q_{pump1}—total flow of SMR pump, m^3/s; η_{Pump1}—coefficient of SMR pump, (COP); $p_{pump1}\left(Q_{pump1}, \omega_{EM1}\right)$—is total SMR pump characteristic; $Q_{L1,1}$—LNG flow in the first section of pipeline, m^3/s.

$$p_{Pump1}\left(Q_{pump1}, \omega_{EM1}\right) = \left(\frac{\omega_{EM1}}{\omega_{EM1,0}}\right)^2 \cdot p_{pump1,0}\left(Q_{pump1,0} = \frac{\omega_{EM10}}{\omega_{EM1}} Q_{L1,1}\right) \quad (14)$$

where $p(Q_{pump1,0})$—total SMR characteristic at an angular velocity $\omega_{EM1,0}$.

Total SMR characteristic is described as a fifth order polynomial with a correlation coefficient of 0.9998 which is determined from points of technical FSRU sheets:

$$p(Q_{pump1,0}) = 5546.7Q^5_{pump1,0} - ump1,0Q^4_{pump1,0} + 473.16Q^3_{pump1,0} - ump1,Q^2_{pump1,0} - ump1,0Q_{pump1,0} + 0.8757 \quad (15)$$

2.6. Description and Mathematical Model of High-Pressure LNG Booster Pumps

Basically, the described electric motor model (EM1) in Section 2.5 can be used for the rest electric motors (EM2, EM3, EM4), though another type of pump is used for LNG transfer. The last step of the LNG transportation system is transferring LNG by a high-pressure booster pump to LNG vaporizers. It is the vertical, cryogenic centrifugal pump. In the FSRU, there are three trains, each consisting of two high-pressure pumps.

Observing the pressure and LNG flow changes through passages of the pump, the model is described by differential equations. These variables have an effect on operational efficiency. The model is shown in Figure 5 below.

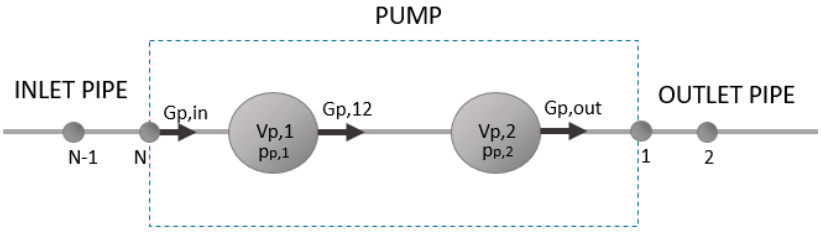

Figure 5. High-pressure booster pump mathematical model. Note: N, N-1—numbers of inlet pipe sections; 1, 2—numbers of outlet pipe sections; Vp,1—the passage between the pipe and the first stage of pump's joint; Vp,2—the passage between the pipe and the second stage of pump's joint; Gp—mass flow of LNG.

Mass flow of LNG ($G_{p,in}$), which enters the passage between the pipe and the first stage of pump's joint, is determined according to differential Equation (16):

$$\dot{G}_{p,in} = \left(\frac{A_{p,in}}{L_{p,in}}\right) \cdot \left[p_N - p_{p,1} - \Delta p_{p,in} \mathrm{sign}(G_{p,in})\right] \quad (16)$$

where $A_{p,in}$—section area between point N and V_{p1}, m^2; $L_{p,in}$—length between point N and $p_{p,1}$, m; p_N—pressure of inlet pipe, Pa; $p_{p,1}$—pressure of the passage between the pipe and the first stage of pump's joint, Pa; $\Delta p_{p,in}$—pressure losses between point N and p_{p1}, Pa; $\mathrm{sign}(G_{p,in})$—sign function, which indicates LNG mass flow direction.

Pressure losses ($\Delta p_{p,in}$) are calculated by Equation (17):

$$\Delta p_{p,in} = 0.5 \cdot \xi_{p,in} \cdot \frac{{G_{p,in}}^2}{\rho_l(p_N){A_{p,in}}^2} \quad (17)$$

Hydraulic losses coefficient ($\xi_{p,in}$) is determined by Equation (18):

$$\xi_{p,in} = \xi_{p,in,local} + \frac{\lambda_{p,in}(Re, \Delta_{p,in})}{8} \quad (18)$$

To calculate hydraulic losses, the $\Delta_{p,in}$ could be determined according to these conditions:

$$\left\{ \begin{array}{c} \lambda_{p,in} = \frac{64}{\sqrt{Re}}, \ when \ Re \le 2320 \\ F(\lambda_{p,in}) = \frac{1}{\sqrt{\lambda_{p,in}}} - 2 \cdot log\left(\frac{2{,}51}{Re \cdot \sqrt{\lambda_{p,in}}} + \frac{\Delta_{p,in}}{3.7 \cdot D_{p,in}}\right) = 0, \ when \ Re \ge 2320 \end{array} \right\} \quad (19)$$

In that case, when LNG flow is turbulent, it could be solved by the Colebrook–White nonlinear algebraic equation $F(\lambda_{p,in}) = 0$ [29,30].

The pressure of the passage between the pipe and the first stage of pump's joint $p_{p,1}$ could be determined by Equation (20):

$$\dot{p}_{p1} = \frac{K\left(p_{p,1}\right)}{V_{p,1}} \cdot \left[\frac{G_{p,in}}{\rho_l\left(p_N\right)} - \frac{G_{p12}}{\rho_l\left(p_{p,1}\right)} \right] \tag{20}$$

where $K\left(p_{p,1}\right)$—bulk modulus of elasticity of LNG, Pa; G_{p12}—LNG mass flow between $p_{p,1}$ and $p_{p,2}$, kg/s; $\rho_l(p_N)$—LNG density in inlet pipe, kg/m^3; $\rho_l\left(p_{p,1}\right)$—LNG density in the passage between the pipe and the first stage of pump's joint, kg/m^3.

LNG mass flow between $p_{p,1}$ and $p_{p,2}$ (G_{p12}) is determined by differential Equation (21) below:

$$\dot{G}_{p12} = \left(\frac{A_{p,12}}{L_{p,12}} \right) \cdot \left[p_{p1} + p_{pump}\left(\omega_{EM}, Q_{p,out}\right) - p_{p,2} - \Delta p_{p12} \mathrm{sign}\left(G_{p12}\right) \right] \tag{21}$$

where Δp_{p12} is determined according to Equation (17).

Having in mind that is the multistage pump, the pump pressure is determined by verifying all stages of the pump, including the pump's characteristics, with Equation (24) below:

$$p_{pump} = N_{stage} \cdot p_{pump,stage}\left(Q_{pump}\omega_{EM}\right) \tag{22}$$

Pump pressure of the one of the stages is determined by Equation (23):

$$p_{pump,stage}\left(Q_{pump}\omega_{EM}\right) = \left(\frac{\omega_{EM}}{\omega_{EM0}}\right)^2 \cdot p_{pump,stage,0}\left(Q_{pump0} = \frac{\omega_{EM0}}{\omega_{EM}} Q_{pout}\right) \tag{23}$$

where $Q_{pout} = \frac{G_{out}}{\rho_l\left(p_{p,2}\right)}$; $p_{pump,stage,0}$—one of the stages of pump's characteristics, which is provided below:

$$p_{pump2,stage} = 8.25511502 \cdot 10^6 - 0.10 \cdot Q_{pump2,0} - 1.523478682 \cdot 10^9 \cdot {Q_{pump2,0}}^2 \tag{24}$$

Pressure ($p_{p,2}$) of the passage between the first stage of the pump's joint and the outlet pipe is determined by:

$$\dot{p}_{p2} = \frac{K\left(p_{p,2}\right)}{V_{p,2}} \cdot \left[\frac{G_{p12}}{\rho\left(p_{p,1}\right)} - \frac{G_{p,out}}{\rho\left(p_{p,2}\right)} \right] \tag{25}$$

where $K\left(p_{p,2}\right)$—bulk modulus of elasticity of LNG, Pa; G_{p12}—LNG mass flow between $p_{p,1}$ and $p_{p,2}$, kg/s; $\rho_l(p_{p,1)}$—LNG density of $Vp_{,1}$, kg/m^3; $\rho_l(p_{p,2)}$—LNG density of $Vp_{,2}$, kg/m^3, $G_{p,out}$—mass flow of LNG from outlet of pump to the outlet pipe, kg/s.

The mass flow of LNG $\left(G_{p,out}\right)$ from outlet of pump to the outlet pipe is determined by Equation (26):

$$\dot{G}_{p,out} = \left(\frac{A_{p,out}}{L_{p,out}} \right) \cdot \left[p_{p,2} - p_{p,1} - \Delta p_{p,out} \mathrm{sign}\left(G_{p,out}\right) \right] \tag{26}$$

where $A_{p,in}$—sectional area between p_{p2} and point 1, m^2; $L_{p,in}$—length between p_{p2} and point 1, m; p_{p1}—pressure of the passage between the pipe and the first stage of pump's joint, Pa; p_{p2}—pressure of the passage between the first stage of the pump's joint and the

outlet pipe, Pa; Δp_{pout}—pressure losses between p_{p2} and point 1, Pa; $\mathrm{sign}(G_{p,out})$—sign function, which indicates LNG mass flow direction.

2.7. System of Equations of the Pipelines Using Method of Characteristics

In the last part of the model, the one-dimensional non-stationary movement of LNG in the variable cross-sectional A(x) area of the pipeline is studied, i.e., when the LNG velocity vector is directed along the axis of a pipeline, and pressure, velocity, and temperature changes in time, and along the axis of the pipeline (coordinate). Moreover, the cross-sectional area A(x) of the pipeline varies and depends on the x coordinates. Furthermore, the flow of LNG in pipes is described by the differential equations of flow integrity and motion with partial derivatives, which are solved by the method of characteristics, and the unknown variables (velocity of LNG, pressure) are determined at every point of the pipeline.

The equation of LNG continuity can be written in a differential form as follows [31–35]:

$$\frac{\partial}{\partial t}[A(x)\rho_l] + \frac{\partial}{\partial x}[A(x)\rho_l \upsilon] = 0 \tag{27}$$

where ρ_l, υ—density and velocity of LNG, kg/m^3 and m/s; $A(x)$ —cross-sectional area of a pipeline, m^2.

Equation of liquid flow impulse (momentum):

$$\frac{\partial}{\partial t}[A(x)\rho_l \upsilon] + \frac{\partial}{\partial t}\left[A(x)\left(p + \rho_l \upsilon^2\right)\right] + \Pi(x)\tau + A(x)\rho_l a_x = p_l \frac{\partial A}{\partial x} \tag{28}$$

where p—LNG pressure, Pa; $\Pi(x)$—the perimeter of cross-section of the pipeline, m; τ—tangential fluid stress on the inner surface of the pipeline, Pa;

$$\tau = \frac{\lambda(Re, \Delta)\rho\upsilon|\upsilon|}{8} \tag{29}$$

where p—LNG pressure, Pa; $\Pi(x)$—the perimeter of a cross-section of the pipeline, m; a_x—the acceleration along the x axis, m^2/s.

$$a_x = g \cdot \sin\alpha \tag{30}$$

where α—angle between horizontal axis and center line of pipe.

The system of Equations (27) and (28) could be expressed according to second-order quasi-linear differential equations:

$$[A]\left\{\frac{\partial u}{\partial t}\right\} + [B(u)]\left\{\frac{\partial u}{\partial x}\right\} = \{f(u)\} \tag{31}$$

where $[A]$, $[B(u)]$—matrices and $\{f(u)\}$—a vector which depends on t, x and elements of a vector $\{u\}^T = [p, v]$ Matrices are described:

$$[A] = \begin{bmatrix} 1 & 0 \\ 0 & 1 \end{bmatrix};\ [B(u)] = \begin{bmatrix} v & c\rho_l{}^2 \\ 1/\rho_l & v \end{bmatrix} \tag{32}$$

Vector is described:

$$\{f(u)\} = \begin{Bmatrix} -\frac{c^2\rho_l v}{S(x)}\frac{\partial A}{\partial x} \\ \frac{\tau\Pi(x)}{A(x)\rho_l} - a_x \end{Bmatrix} \tag{33}$$

where c—speed of sound in the LNG, m/s.

By equating the determinant of the matrix $[B(u)] - [A]\frac{dx}{dt}$ to zero, which allows determining the $\frac{dx}{dt}$ derivative and determines characteristic direction. This equation has two various real roots: $\frac{dx}{dt} = \lambda_i$, $(i = 1.2)$

$$C^+ : \frac{dx}{dt} = \upsilon + c;\ C^- : \frac{dx}{dt} = \upsilon - c \tag{34}$$

Such liquid movement is characterized by the wave of increased and reduced pressure, which spreads from the place of change in each pressure vibration cross-section and in the deformation of high-pressure pipeline walls [36,37]. The speed of sound c in the LNG, which is stored in the pipeline, is equal to:

$$c = \sqrt{\frac{\frac{K(p,T)}{\rho_l}}{1 + \frac{K(p,T)\cdot D_{in}}{E\cdot e}}} \tag{35}$$

where $K(p,T)$—bulk modulus of elasticity of liquid, Pa; $K(p,T) = \rho_l \frac{dp}{d\rho_l}$; ρ_l—density of the LNG; E—modulus of elasticity of a pipeline, Pa; D_{in}—internal diameter of a pipeline, m; e − thickness of a wall of a pipeline, m.

The main idea of the characteristics method (MOC) is the fact that the unknown variable velocity (v) and the pressure of the liquid (p) at an instant moment time t + Δt are determined according to the parameters that time t + Δt [29,38]. The MOC scheme is shown in Figure 6.

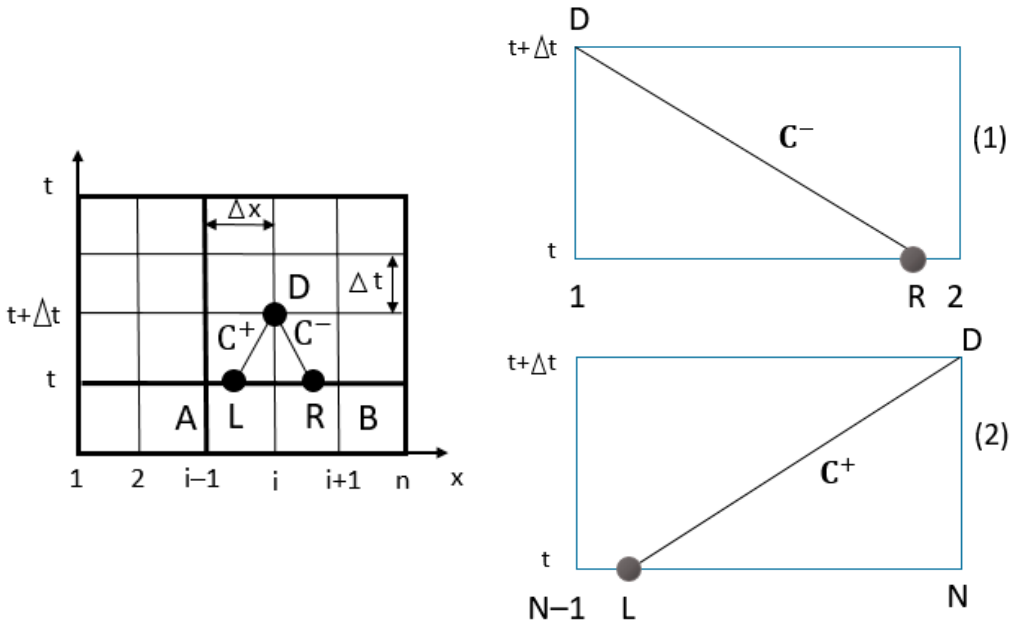

Figure 6. Method of characteristics (**a**) Schematic of characteristic line for MOC; (**b**) Calculation schemes of the first and the last points.

Pressure and velocity at point D at that moment of time are determined from a nonlinear algebraic equation system:

$$C^+ : \Phi_1 = v_D - v_D + \tfrac{1}{2}(\rho_D - \rho_L)\left[\left(\tfrac{1}{\rho_l c}\right)_L + \left(\tfrac{1}{\rho_l c}\right)_D\right] - \tfrac{\Delta t}{2}\left[\left(\tfrac{f_1}{\rho_l c}\right)_L + \left(\tfrac{f_1}{\rho_l c}\right)_D\right] - \tfrac{\Delta t}{2}[(f_2)_L + (f_2)_D] = 0 \tag{36}$$

$$C^{-}: \Phi_2 = v_D - v_R + \frac{1}{2}(\rho_D - \rho_R)\left[\left(\frac{1}{\rho_l c}\right)_R + \left(\frac{1}{\rho_l c}\right)_D\right] - \frac{\Delta t}{2}\left[\left(\frac{f_1}{\rho_l c}\right)_R + \left(\frac{f_1}{\rho_l c}\right)_D\right] - \frac{\Delta t}{2}[(f_2)_R + +(f_2)_D] = 0 \quad (37)$$

where $f_1(p, \upsilon) = \frac{c}{S(x)}\left(\rho_l \upsilon \frac{\partial S}{\partial x}\right)$; $f_2(\upsilon, p) = \frac{\tau \Pi(x)}{\rho_l S(x)}$.

The nonlinear algebraic Equations (36) and (37) are solved by the Newton and Raphson method [39]:

$$[J]_{i-1}\{\Delta Y\}_i = -\{\Phi\}_{i-1};\ \{Y\}_i = \{\Delta Y\}_{i-1} + \{\Delta Y\}_i \quad (38)$$

$$[J]_{i-1} = \begin{bmatrix} \frac{\partial \Phi_{1,i-1}}{\partial p} & \frac{\partial \Phi_{1,i-1}}{\partial v} \\ \frac{\partial \Phi_{2,i-1}}{\partial p} & \frac{\partial \Phi_{2,i-1}}{\partial v} \end{bmatrix};\ \{\Delta Y\}^T{}_i = [\Delta p_i,\ \Delta v_i];\ \{\Phi\}^T_{i-1} = [\Phi_{1,i-1}, \Phi_{2,i-1}] \quad (39)$$

where $[J]_{i-1}$ — Jacobi matrix; $\{\Delta Y\}_i$— increment vector of unknown variables; i—number of iterations.

To ensure the stability of the solution, the Courant–Friedrichs–Lewy condition shall be fulfilled [40]:

$$\frac{\Delta t|v + c|}{\Delta x} \le C_r \quad (40)$$

where C_r is Courant number.

At points L and R, variables p and v are defined using a system of two nonlinear algebraic equations with unknown $p_{L,}$ $v_{L,}$ and p_R, v_R:

$$\Phi_3 = p_L - p_C - \theta(p_A - p_C)[v_L + c(p_L)] = 0 \quad (41)$$

$$\Phi_4 = v_L - v_C - \theta(v_A - v_C)[v_L + c(p_L)] = 0 \quad (42)$$

And

$$\Phi_5 = p_R - p_C + \theta(p_B - p_C)[v_R - c(p_R)] = 0 \quad (43)$$

$$\Phi_6 = v_R - v_C + \theta(v_B - v_C)[v_R - c(p_R)] = 0 \quad (44)$$

where $= \frac{\Delta t}{\Delta x}$.

The boundary conditions are used to connect the pipeline with the equipment of the system (LNG tank, Suction Drum, pumps, etc.), which are described below:

1. Boundary condition: when the point is known $x = 0$, pressure is known variable $p(t) = p_D$, then LNG flow velocity is determined by formula:

$$\Phi_2(v_D) = 0 \quad (45)$$

2. Boundary condition: when the point is known $x = 0$, LNG flow velocity is known variable $v(t) = v_D$, then pressure is determined by formula:

$$\Phi_2(p_D) = 0 \quad (46)$$

3. Boundary condition: when the point is known $x = L$, pressure is known variable $p(t) = p_D$, then LNG flow velocity is determined by formula:

$$\Phi_1(v_D) = 0 \quad (47)$$

4. Boundary condition: when the point is known $x = L$, NG flow velocity is known variable $v(t) = v_D$, then pressure is determined by formula:

$$\Phi_1(p_D) = 0 \quad (48)$$

When boundary conditions are set according to Equations (45) and (48), the nonlinear algebraic equations are solved by the Newton and Raphson method. Then, the Pipeline Unit (Volume—V3) is used to determine one of the last unknown variables—pressures (Figure 7).

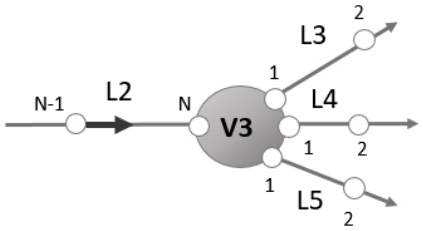

Figure 7. Pipeline Unit V3 connection with pipes (L2, L3, L4, L5). Note: see in Figure 1.

At the Pipeline Unit (V3), the LNG flow balance equation is written to determine the pressure:

$$\dot{p}_{V3} = \frac{K(p_{V3},T)}{V3}\left(Q_{L2,N})sign(Q_{L2,N}) - Q_{L3,1}sign(Q_{L3,1}) - Q_{L4,1}sign(Q_{L4,1}) - Q_{L5,1}sign(Q_{L5,1}) - Q_{Losses}sign(p_{V3})\right) \quad (49)$$

where $Q_{L2,N}$, $Q_{L3,1}$, $Q_{L4,1}$, $Q_{L5,1}$, Q_{Losses}—LNG volume flow, m^3/s; $Q_{Losses}(p_{V3})$–losses of LNG volume flow, m^3/s.

Velocities of LNG in Pipeline Unit sections of pipes L2, N and L3,1, L4,1, and L5,1 are determined when pressure is known in the Pipeline Unit (V3), using boundary conditions (45), (47) by:

$$\begin{aligned} C^+ &: \Phi_1(p_{V3}, v_{L2,N}) = 0 \\ C^- &: \Phi_2(p_{V3}, v_{L3,1}) = 0 \\ C^- &: \Phi_2(p_{V3}, v_{L4,1}) = 0 \\ C^- &: \Phi_2(p_{V3}, v_{L5,1}) = 0 \end{aligned} \quad (50)$$

For mathematical model construction, there are two important conditions:

(a) When pipes (L3, L4, L5) are closed until HP booster pump 1 starts working:

$$\begin{aligned} C^+ &: \Phi_1(p_{L3}(x = L3), v_{L3-end} = 0) \\ C^+ &: \Phi_1(p_{L4}(x = L4), v_{L4-end} = 0) \\ C^+ &: \Phi_1(p_{L5}(x = L5), v_{L5-end} = 0) \end{aligned} \quad (51)$$

(b) When HP booster pump 1 starts working and pipes start opening:

$$\begin{aligned} C^+ &: \Phi_1\left(p_{L3}(x = L3), v_{L3-end} = \frac{G_{p,in}}{A_{p,in}\cdot\rho_l}\right) \\ C^+ &: \Phi_1\left(p_{L4}(x = L4), v_{L4-end} = \frac{G_{p,in}}{A_{p,in}\cdot\rho_l}\right) \\ C^+ &: \Phi_1\left(p_{L5}(x = L5), v_{L5-end} = \frac{G_{p,in}}{A_{p,in}\cdot\rho_l}\right) \end{aligned} \quad (52)$$

Finally, the model is finished in the LNG transfer to the BOG recondensers. The velocity of LNG in Pipeline Unit sections of pipes L6, L7, and L8 are determined when pressure is known, using boundary conditions (47) by:

$$\begin{aligned} C^+ &: \Phi_1(p_{L6}(x = L6), v_{L6-end}) = 0 \\ C^+ &: \Phi_1(p_{L7}(x = L7), v_{L7-end}) = 0 \\ C^+ &: \Phi_1(p_{L8}(x = L8), v_{L8-end}) = 0 \end{aligned} \quad (53)$$

The pressure at the end of the pipes L6, L7 and L8 is determined according to the expression below:

$$p_{Lk}(x = Lk) = 0.5 \cdot \xi_{Lk-end} \cdot v_{Lk-end}{}^2 + p_{Lk,0} \quad (54)$$

where $p_{Lk,0}$—constant pressure in the pipes.

Hydraulic losses coefficient:

$$\xi_{Lk} = \left[\left(\frac{A_{Lk}}{n_{channel,k} \cdot A_{channel,k}} \right)^2 - 1 \right] \quad (55)$$

where pipe index—k = 6, 7, 8 and A_{Lk}—cross-section area of pipe k, m^2; $A_{channel,k}$—cross-section area of channel of k-th BOG recondenser, m^2; $n_{channel,k}$—number of channels of k-th BOG recondenser.

All in all, the theoretical mathematical model was built for the full LNG transportation system in the FSRU in this section. A general mathematical model of the system is released with a special software package using Fortran programing language and MATLAB R28a.

3. Results of LNG Transportation System Dynamics and Hydrodynamics Processes

A mathematical model of the FSRU LNG transportation system was created to solve total system equations with different boundary conditions and determine the final system parameters, such as pressure and velocity. In the mathematical model, the solution time step is 10^{-5} s, and the discretization step of the pipes is 0.1 m. The total solution time is chosen as 5 s. The temperature of LNG in the LNG tank, the Suction Drum, and the pipelines is 110 K. The general conditions of FSRU equipment when the LNG transportation system starts working are summarized in Table 2.

Table 2. Specifications of FSRU equipment.

Equipment	Specification
LNG Tank	Maximum liquid level: 27 m. Cross-section area: 78 m^2.
Submerged Motor Cargo Pump	Maximum capacity: 550 m^3/h. Electric motor power: 132 kW. Mass inertial moment of electric motor rotor: 1.5 kg/m^2. Mass inertial moment of pump wheel: 13 kg/m^2.
Suction Drum	Maximum liquid level: 5 m. Cross-section area: 27 m^2.
High-Pressure Booster Pump	Maximum capacity: 510 m^3/h. Electric motor power: 1000 kW. Mass inertial moment of pump rotor: 13. Mass inertial moment of electric motor rotor: 21 kg/m^2. Mass inertial moment of pump wheel: 13 kg/m^2.
BOG Recondensers (Heat Exchangers)	Number of channels (from pipe L6, 600,000. Number of channels (from pipe L7): 650,000. Number of channels (from pipe L8): 700,000.

Table 3 lists different diameters and lengths or angles of inclination of pipes and pipelines considered in the simulation of LNG flow. Before starting the mathematical model simulation, it is essential to mention that in this model, that LNG flow transfers at different diameters and lengths or tilt angles of pipes and pipelines (described in Table 2), presenting better results and the universality of the model.

Table 3. Specification of FRSU LNG transportation pipelines system.

Pipe	Name	Diameter, m	Length, m	Tilt Angle
Pipeline from the LNG tank to the Suction Drum (L1)				
	L1,1	0.40	4	0
	L1,2	0.40	10	90
	L1,3	0.40	63	180
	L1,4	0.50	10	180
	L1,5	0.60	11	180
	L1,6	0.50	104	180
	L1,7	0.20	20	270
	L1,8	0.20	2	0
Pipeline from the Suction Drum to the Pipeline Unit (L2)				
	L2,1	0.40	1	270
	L2,2	0.40	1	0
	L2,3	0.40	2	90
Pipe from the Pipeline Unit to the HP Booster Pump 1	L3	0.20	1	0
Pipe from the Pipeline Unit to the HP Booster Pump 2	L4	0.20	1	0
Pipe from the Pipeline Unit to the HP Booster Pump 3	L5	0.20	1	0
Pipe from the HP Booster Pump 1 to the BOG recondenser 1	L6	0.20	2	0
Pipe from the HP Booster Pump 2 to the BOG recondenser 2	L7	0.20	2	0
Pipe from the HP Booster Pump 3 to the BOG recondenser 3	L8	0.20	2	0

The model simulation began when the SMR pump with an electric motor (EM1) started working. Figure 8 represents the angular velocity of electric motors and how fast the orientation of pumps changes with the solution time. Additionally, it firstly shows that that EM1 of the SMR pump starts working, indicated by the blue line. Then the second electric motor of HP Booster Pump 1 (EM2) turns on after 0.5 s (red-color curve), the electric motor of HP Booster Pump 2 (EM3) turns on after 1.0 s (yellow-color curve), and the last electric motor of HP Booster Pump 3 (EM4) starts after 1.5 s (purple-color curve).

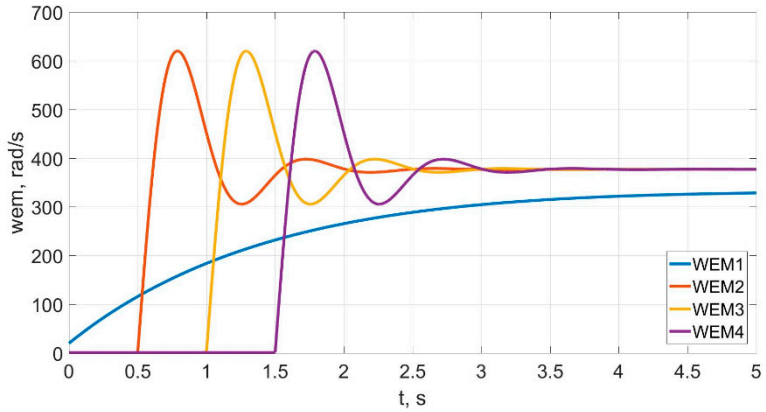

Figure 8. Angular velocity of electric motors: EM1, EM2, EM3, EM4.

In general, the observation of pressure and velocity simulated by the mathematical model in the first LNG pipeline of the LNG transportation system agrees well with the technical data. Figure 9a shows the initial pressure curve along the pipeline L1 (from the LNG tank to the Suction Drum) after the start of the system, and Figure 9b shows pressure

change for 5 s in the first pipeline. Furthermore, the observation of pressure and velocity was selected in the different pipeline distances, using different color lines to verify pipeline geometry. After 4 s, it can be seen that pressure and velocity start to stabilize (Figure 9d).

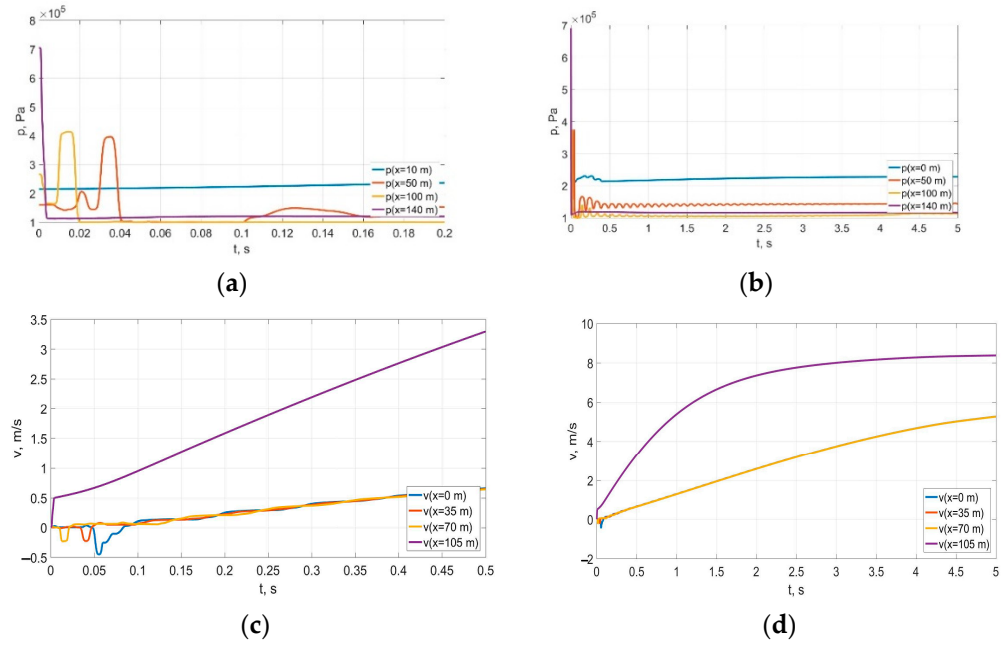

Figure 9. Pressure and velocity in the 1st pipeline (L1) (Table 2) of the LNG transportation system. Note: (**a**) pressure observation when the system starts working; (**b**) pressure observation during simulated solution time in the first pipeline in the LNG transportation system; (**c**) velocity observation when the system starts working; (**d**) velocity observation during simulated solution time in the first pipeline in the LNG transportation system.

After solving (1)–(5) equations of the LNG level in the LNG transportation system, after the solution time run, the results showed that level of LNG decreases in the LNG tank (Figure 10a) and it starts slowly filling with LNG in the Suction Drum (Figure 10b). The filling level in the Suction Drum increases by 0.040 m in the first second of the simulation time before the filling level continuously decreases by approximately 0.030 m per second, as in the main LNG tank (about 0.025 m per 1.7 s simulation time).

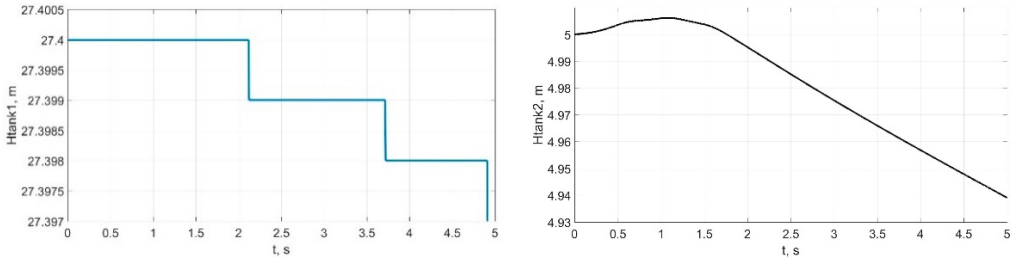

Figure 10. LNG level observation from the beginning to the end of solution time: (**a**) in the LNG tank; (**b**) in the Suction Drum.

Figure 11 indicates the results of simulated pressure in the second pipeline (L2). Observing hydrodynamic processes verifies that the pressure and velocity of L2 depend on the start-up time moment of HP Booster Pumps. Figure 11a, during 0.4–0.5 s, shows pressure waves in the LNG, indicating that pipes L3, L4, and L5 are closed and that the systems work only in the Suction Drum. Comparing Figure 10b (LNG level in the Suction Drum) and Figure 11a, it can be seen that a moment after 0.8 s that HP Booster Pump 1 starts

working, LNG is transported by it in the further system (pipeline L2, Pipeline Unit V3). However, it is verified that the HP Booster Pumps 2 and 3 do not work.

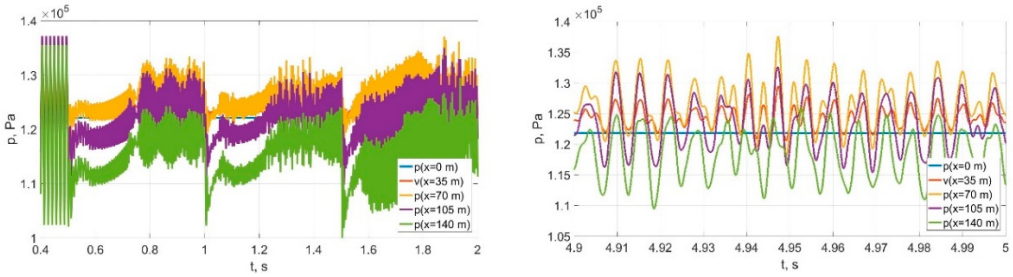

(**a**) (**b**)

Figure 11. Pressure in the 2nd pipeline (L2) (Table 2) of the LNG transportation system: (**a**) the beginning of the simulation time; (**b**) the end of the simulation time.

Meanwhile, Figure 11b shows pressure pulsation in the pipeline (L2) when all the HP Booster Pumps start working. The diagram of Figure 11b estimates that pressure in pipeline 2 changes at a frequency of about 160 Hz and is influenced by HP Booster Electric Motor 1 and pressure wave propagation velocity in part of the system (L2, L3, L6, and other L7, L8 pipes are closed). The pressure pulsation indicated that the system was ready to work for further regasification process. The pulsations of pressure are important to observe because they could load pipes, i.e., the stresses in the pipe walls start increasing, which affects the creation of cracks and the occurrence of material defects inside layers of contact [41].

Figure 12 shows pressure changes in the Pipeline Unit (Volume—V3). Figure 12a shows when HP Booster Pumps turn on (peaks): after 0.5 s—the first HP booster pump; after 1 s—the second HP booster pump; and after 1.5 s—the third HP booster pump. The pumps' work indicates that the further step would be the LNG regasification process. Figure 12b shows that pressure changes are slightly similar to those in the pipeline (L2). As Figure 12b shows, there is pressure pulsation in the whole system.

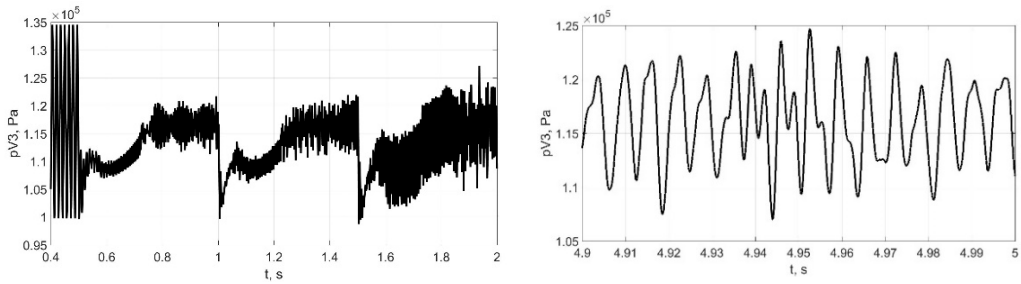

(**a**) (**b**)

Figure 12. Pressure in the Pipeline Unit of the LNG transportation system: (**a**) the beginning of the simulation time; (**b**) the end of simulation.

Figure 13 shows the mass flow of the LNG of HP Booster Pumps to the outlet pipes. Figure 13a introduces the beginning of HP Booster Pump work. At the end of the solution time (5 s), the flow rate is approximately 502 m^3/h for HP Booster Pumps (Figure 13b). The estimated mass flow is based on Equations (16), (21) and (27), which are related to pressure and velocity changes. Additionally, it is important to mention that the analyzed LNG transportation system is completely closed and constantly operating (isolated from the environment). So, the average values of some of the main technical parameters could only be observed over a certain period of time. For example, to compare the flow: in our theoretical studies of the real system, it has an average value of 502 m^3/h, compared to the real system according to the technical parameters, the value is 520 m^3/h. A slight difference

in LNG flow is because we preferred to study the hydrodynamic processes occurring in pipes L6, L7 and L8 under different boundary conditions, i.e., on the number of tubes of varying heat exchangers (which leads to different pressure losses).

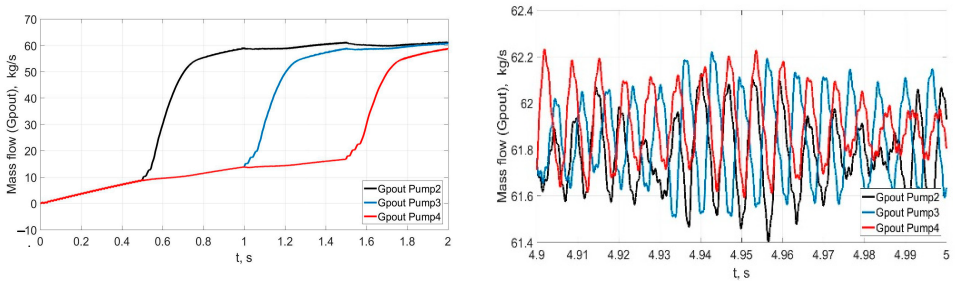

Figure 13. Mass flows of LNG of HP Booster Pumps: (**a**) the beginning of the simulation time; (**b**) the end of the simulation.

To finalize the LNG transportation process, the last parameters of hydrodynamics were verified (pressure and velocity). Figure 14 shows LNG pressure and velocity changes in pipes 6, 7 and 8 when HP Booster Pumps turn on at different times and start working. After 5 s, we observed pulsations pressure and velocity (Figure 14b). The many pulsation peaks with different amplitudes show an unsteady flow of LNG. Due to the unsteady LNG flow, LNG flow monitoring is important for further analysis of LNG vaporization in heat exchangers. Vaporization efficiency depends on pressure, temperature, mass flow, and volume fraction changes. From the research of [31], we take that an FSRU is a complicated system with various heat transfer mechanisms and has actual demands of improving efficiency and compactness.

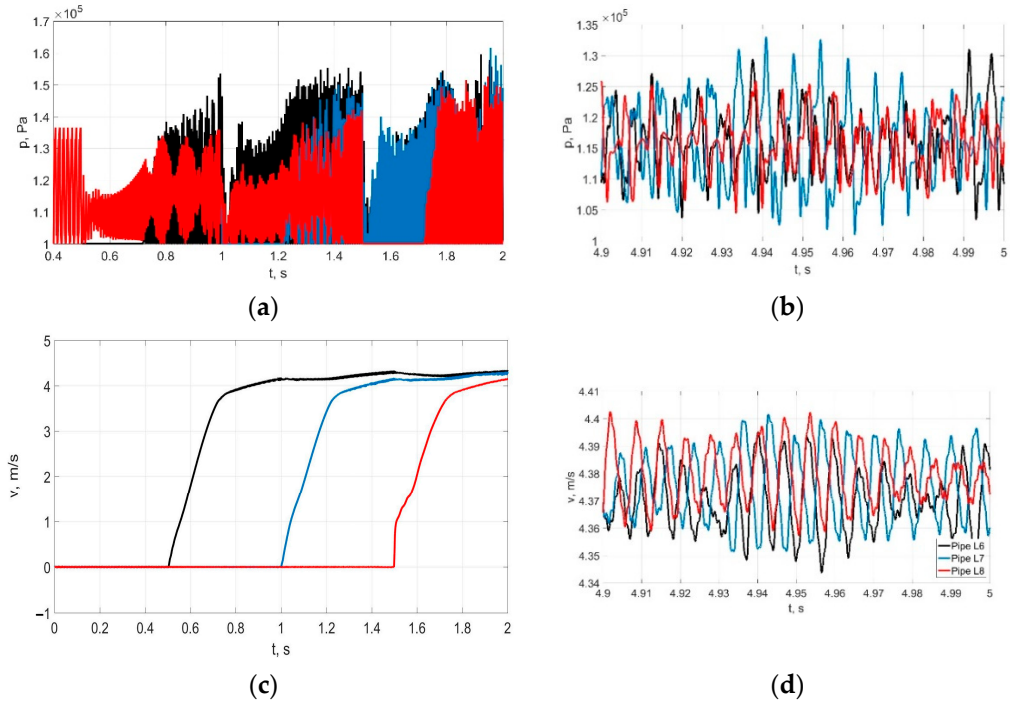

Figure 14. Pressure in the 6th, 7th, and 8th pipes (Table 2) of the LNG transportation system: Note: (**a**) Pressure observation when the system starts working; (**b**) Pressure observation at the end of the solution time; (**c**) Velocity observation when the system starts working; (**d**) Velocity observation at the end of the solution time.

Figure 15 introduces pressure and velocity changes in the sixth pipe. Figure 15a shows that the HP Booster Pump starts working after 0.5 s, so the pressure suddenly increases. Hydrodynamic processes did not stabilize because of pressure waves in the LNG. It could be seen from Figure 15b that pressure pulsation is smaller at the end of the pipe because of the boundary conditions input, and that pressure depends on velocity (see green line in Figure 15b). However, at other points of the pipe, pressure pulsation is bigger (other color lines) because of the pressure losses along the L6 pipe. Furthermore, it is seen from Figure 15c that velocity varies similarly to pressure in the pipe. At the end of solution time (5 s), the LNG average velocity reaches approximately 4.37 m/s (Figure 14d).

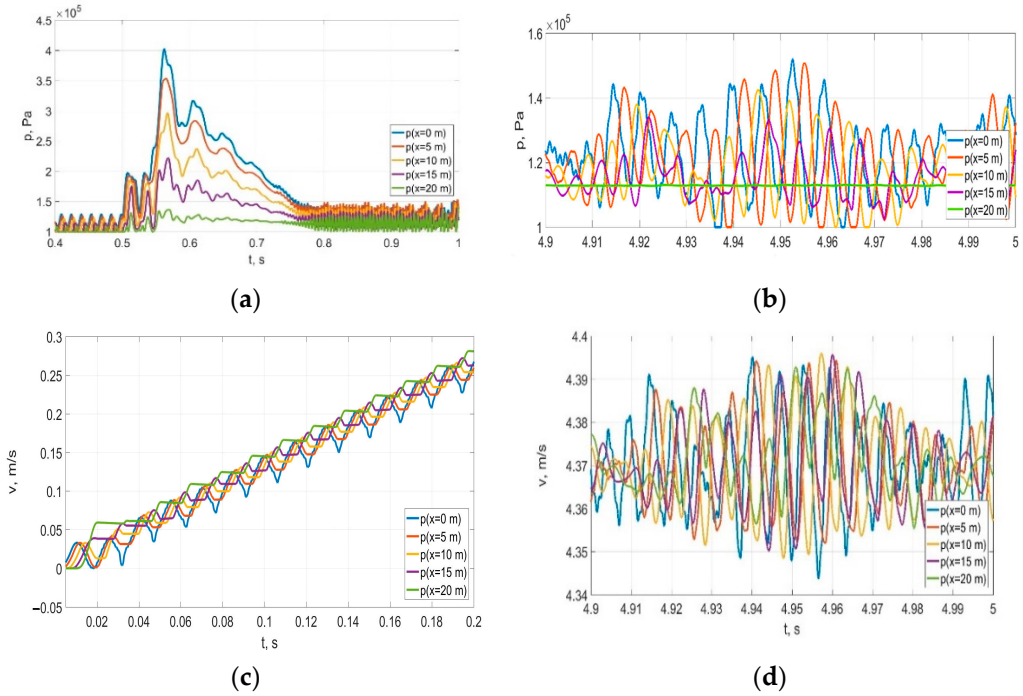

Figure 15. Pressure in the 6th pipe (L6) (Table 2) of the LNG transportation system: Note: (**a**) Pressure observation when the system starts working; (**b**) Pressure observation at the end of the solution time; (**c**) Velocity observation when the system starts working; (**d**) Velocity observation at the end of the solution time.

The variation of hydrodynamic processes (pressure and velocity) at any time is presented at the system's characteristic points, which indicates curves of different colors in Figures 9, 11 and 15. These curves show different pressure and velocity changes at other points and at each time. As mentioned in the introduction, these pressure and velocity changes are important for safe and reliable FRSU operations without compliances, especially in holding mode, LNG transporting between tanks, the regasification process, and the ship-to-ship procedure.

Figure 16 introduces hydraulic energy losses in the first (Figure 16a) and the rest of the other pipes of the LNG transportation system (Figure 16b). Hydraulic energy losses (power of hydraulic friction forces) depend on LNG velocity, length and inner diameter of the pipe, and roughness of the inside surface of the pipe. So, it can be seen from Figure 16a that the highest energy losses are in the first pipeline due to the different geometric parameters of the pipeline—diameter, tilt angle, and length.

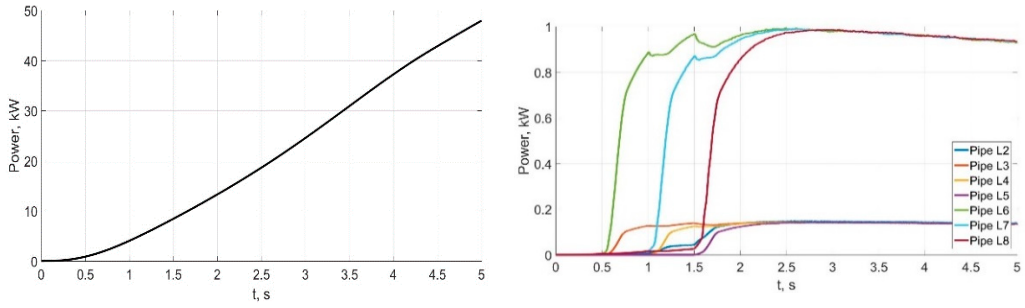

(**a**) (**b**)

Figure 16. Hydraulic energy losses. Note: (**a**) Hydraulic energy losses in the 1st pipeline (L1); (**b**) Hydraulic energy losses in all pipelines and pipes.

After 5 s, hydraulic energy losses in the pipe L1 are equal to 50 kW, respectively, and total energy equals 53 kW. These hydraulic energy losses in all pipes contain 1.7% of the whole system power (total power of the electric motors is 3132 kW). In Figure 16b, we can observe hydraulic energy losses in different pipes or pipelines, which is important for another regasification process. This mathematical model of total system would help control energy losses in the FSRU (LNG Terminal of Klaipeda City, Lithuania) in various technological modes.

The model validation was performed using technical data in daily intervals, as is typical for FSRUs. For the individual components of the model, such as the pumps, combined with the pump and electrical characteristics from manufacturers, we were able to generate curves at various angular velocities, as shown in Figure 17.

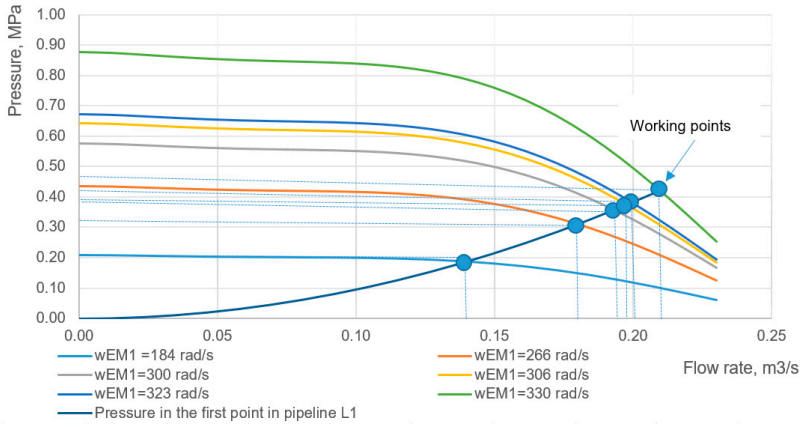

Figure 17. Curves at various angular velocities for the main pump (SMR pump Model SMR 200; see Figure 8) as a component of the presented model.

Figure 17 shows how the SMR pump generates pressure as a function of our angular velocity. For comparison, the lowest blue curve from Figure 8 shows the operating points, i.e., the dependence of the pressure on the flow rate of the first line (L1,1) at the first point. The electric motor is connected to the pump, and using the manufacturer's pump curve p(Q) at different motor angular velocity $\omega_{EM1}(t)$, we obtain the pump curve $p_{Pump1}\left(Q_{pump1}, \omega_{EM1}\right)$ at the corresponding motor angular velocity $\omega_{EM1}(t)$. This gives the pressure generated by the real pump in the system.

In the model, all devices connect to one system, so when changing pressure, speed, or other parameters, other parameters of the system change as well (the system works automatically). According to the manufacturer's technical data, the model does not work in any mode other than the one set. Therefore, we can assume the validity of the model in the simulated time range in seconds, although naturally, for an FSRU there are no technical

values in this time scale. The uniqueness of our model is that the parameters and the linking algorithm are fixed at a 5 s interval at the start time for each point of the system.

4. Conclusions

This research investigates the hydrodynamics and dynamics processes in the real LNG transportation system of FSRUs (LNG Terminal of Klaipeda City) in system start-up (until 5 s) mode. The created total mathematical model of the LNG transportation system consists of electric motors, pumps, tanks, and pipelines, enabling the evaluation of electric motors, pumps' dynamics characteristics, and speed of sound in the LNG when LNG flow enters the LNG regasification unit.

Using this model, it is possible to study various technological regimes (for example, starting pumps at different times and varying the initial height of filling tanks with liquid). The model simulation began when the SMR pump with an electric motor (EM1) started working. The results of the study of hydrodynamic processes are obtained when the second electric motor of HP Booster Pump 1 (EM2) is started after 0.5 s, the third electric motor of HP Booster Pump 2 (EM3) is started after 1.0 s, and the fourth electric motor of HP Booster Pump 3 (EM4) is started after 1.5 s, after the first pump is started.

The hydrodynamic processes in the considered system have not yet been steady after 5 s. During the test time of 5 s, the pressures and velocities in pipe 6 change at a frequency of about 160 Hz, which depends on the rotation of electric motors, LNG physical and mechanical properties, and the materials of pipes.

We can accurately characterize the flow parameters (velocity, pressure) entering the additional regasification equipment (LNG vaporizers) with this model. For example, our theoretical studies of the real system obtained an average value of 502 m^3/h, compared to the real system according to the technical parameters, with a value of 520 m^3/h. The slight difference in LNG flow is because we additionally preferred to study the hydrodynamic processes occurring in pipes L6, L7 and L8 under different boundary conditions, i.e., the number of tubes of different heat exchangers (which leads to different pressure losses).

Hydraulic energy losses (power of hydraulic friction forces) depend on LNG velocity, length and inner diameter of the pipe, and roughness of the inside surface of the pipe. It was found that hydraulic energy losses in all pipes were equal to 53 kW. These hydraulic energy losses in all pipes contain 1.7% of the whole system power (the total power of the electric motors is 3132 kW). It was determined that a slight variation in LNG temperature does not significantly affect the hydrodynamic processes in the system.

In general, the pressure and velocity results of the mathematical model agree well with the technical data, which also confirms that the mathematical model is suitable to characterize real technological regimes of regasification in Floating Storage and Regasification Systems. The model found that the LNG flow in this system is unsteady and should be monitored for further regasification processes.

Author Contributions: Conceptualization, V.S. and M.B.; methodology, V.S. and M.B.; software, V.S., M.B. and A.D.; validation, M.B. and V.S.; formal analysis, V.S., M.B. and A.D.; investigation, V.S. and M.B.; resources, V.S. and T.P.; data curation, V.S. and M.B.; writing—original draft preparation, V.S., J.U. and M.B.; writing—review and editing, T.P. and J.U.; visualization, V.S. and M.B.; supervision, V.S. and M.B.; project administration, V.S. and M.B.; funding acquisition, T.P. and V.S. All authors have read and agreed to the published version of the manuscript.

Funding: This research received no external funding.

Institutional Review Board Statement: Not applicable.

Informed Consent Statement: Not applicable.

Data Availability Statement: All data generated or analyzed during this study are included in this published article.

Conflicts of Interest: The authors declare no conflict of interest.

References

1. European Commission. The European Green Deal, Brussels 2019. Available online: https://ec.europa.eu/info/sites/default/files/european-green-deal-communication_en.pdf (accessed on 5 September 2022).
2. DNV GL AS. Technology Outlook 2025. Norway 2016. Available online: https://brandcentral.dnv.com/fileroot/gallery/dnvgl/files/original/4f01c13e94af4438b971c5254b7d8664/4f01c13e94af4438b971c5254b7d8664_low.pdf (accessed on 5 September 2022).
3. International Gas Union. World LNG Report 2022. IGU 2022. Available online: https://www.igu.org/resources/world-lng-report-2022/ (accessed on 5 September 2020).
4. Statistical Review of World Energy. BP, London 2020. Available online: https://www.bp.com/content/dam/bp/business-sites/en/global/corporate/pdfs/energy-economics/statistical-review/bp-stats-review-2020-full-report.pdf (accessed on 5 September 2020).
5. Wang, C.; Ju, Y.; Wang, T.; Zou, S. Transient performance study of high pressure fuel gas supply system for LNG fueled ships. *Cryogenics* **2022**, *125*, 103510. [CrossRef]
6. Bosser, L.; Moreno, G. The TEN-T Review: A Welcome but Perfectible Proposal. Conference of Peripheral Maritime Regions, 2022. Available online: https://cpmr.org/wpdm-package/the-ten-t-review-a-welcome-but-perfectible-proposal/ (accessed on 5 September 2020).
7. Ren, J.; Liang, H. Measuring the sustainability of marine fuels: A fuzzy group multi-criteria decision making approach. *Transp. Res. Part D Transp. Environ.* **2017**, *54*, 12–29. [CrossRef]
8. International Gas Union. World LNG Report. IGU 2020. Available online: https://www.igu.org/resources/2020-world-lng-report/ (accessed on 5 September 2020).
9. Semaskaite, V.; Bogdevicius, M.; Paulauskiene, T.; Uebe, J.; Filina-Dawidowicz, L. Improvement of Regasification Process Efficiency for Floating Storage Regasification Unit. *J. Mar. Sci. Eng.* **2022**, *10*, 897. [CrossRef]
10. Khan, M.S.; Wood, A.D.; Qyyum, A.M.; Ansari, K.B.; Ali, W.; Wazwaz, A.; Dutta, A. Graphical approach for estimating and minimizing boil-off gas and compression energy consumption in LNG regasification terminals. *J. Nat. Gas Sci. Eng.* **2022**, *101*, 104539. [CrossRef]
11. The American Bureau of Shipping. *LNG Bunkering: Technical and Operational Advisory*; The American Bureau of Shipping: Houston, TX, USA, 2015; pp. 8–65. Available online: https://superlng.adrioninterreg.eu/wp-content/uploads/2020/04/2_FILE.pdf (accessed on 7 September 2020).
12. Andreev, A.M.; Baranov, A.Y.; Sokolova, E.V.; Malysheva, T.A.; Ivanov, L.V. Selection of technological solutions to reduce LNG loss in supply pipelines to LNG terminal. *AIP Conf. Proc.* **2021**, *2412*, 030023. [CrossRef]
13. Koo, B. A novel implicit method of characteristics using pressure-referenced correction for transient flow in natural gas pipelines. *J. Nat. Gas Sci. Eng.* **2022**, *104*, 104665. [CrossRef]
14. Li, J.; Hu, H.; Wang, H. Numerical investigation on flow pattern transformation and heat transfer characteristics of two-phase flow boiling in the shell side of LNG spiral wound heat exchanger. *Int. J. Therm. Sci.* **2020**, *152*, 106289. [CrossRef]
15. Pan, J.; Wang, J.; Tang, L.; Bai, J.; Lia, R.; Lub, Y.; Wua, G. Numerical investigation on thermal-hydraulic performance of a printed circuit LNG vaporizer. *Appl. Therm. Eng.* **2020**, *165*, 114447. [CrossRef]
16. Bai, J.; Pan, J.; He, X.; Wang, K.; Tang, L.; Yang, R. Numerical investigation on thermal hydraulic performance of supercritical LNG in sinusoidal wavy channel based printed circuit vaporizer. *Appl. Therm. Eng.* **2020**, *175*, 115379. [CrossRef]
17. Zhao, Z.; Zhao, K.; Ji, D.; Jiang, P.; Shen, R. Numerical Investigation on the Flow and Heat Transfer Characteristics of Supercritical Liquefied Natural Gas in an Airfoil Fin Printed Circuit Heat Exchanger. *Energies* **2017**, *10*, 1828. [CrossRef]
18. Karyakina, E.D.; Shammazov, I.A.; Shalygin, A.V. Main aspects of liquefied natural gas process line thermal and hydraulic calculations. *IOP Conf. Ser. Earth Environ. Sci.* **2021**, *677*, 052056. [CrossRef]
19. Zhmakin, V.; Samoylov, A. Study of two-phase transportation mode of liquefied natural gas through a pipeline by the gravitational method. *IOP Conf. Ser. Mater. Sci. Eng.* **2021**, *1138*, 012047. [CrossRef]
20. Migliore, C.; Tuvilleja, C.; Vesovic, V. Weathering prediction model for stored liquefied natural gas (LNG). *J. Nat. Gas Sci. Eng.* **2015**, *26*, 570–580. [CrossRef]
21. Huerta, F.; Vesovic, V. A realistic vapour phase heat transfer model for the weathering of LNG stored in large tanks. *Energy* **2019**, *174*, 280–291. [CrossRef]
22. Krikkis, R.N. A thermodynamic and heat transfer model for LNG ageing during ship transportation. Towards an efficient boil-off gas management. *Cryogenics* **2018**, *92*, 76–83. [CrossRef]
23. Tietz, C.; Richter, M.; Kleinrahm, R.; Span, R. Enhancement of the revised Klosek and McKinley method for density calculations of liquefied natural gas (LNG) over the temperature range from (100 to 135) K at pressures up to 10 MPa. *Fuel Process. Technol.* **2017**, *165*, 19–26. [CrossRef]
24. GIIGNL. *Custody Transfer Handbook*, 5th ed.; International Group of Liquefied Natural Gas Importers: Neuilly sur Seine, France, 2017; pp. 1–179. Available online: https://giignl.org/system/files/giignl_cthb_5.0.web_.pdf (accessed on 1 October 2020).
25. Shinko Ind. Ltd. Technical Sheet of Submerged Motor Pump, 2017. Available online: https://www.shinkohir.co.jp/pdf/catalog/SM.pdf (accessed on 7 September 2020).
26. Wang, C.; Zhang, Y.; Hou, H.; Zhang, J.; Xu, C. Entropy production diagnostic analysis of energy consumption for cavitation flow in a two-stage LNG cryogenic submerged pump. *Int. J. Heat Mass Transf.* **2019**, *129*, 342–356. [CrossRef]
27. Mokhatab, S.; Poe, W.; Mak, J. *Handbook of Natural Gas Transmission and Processing*, 3rd ed.; Elsevier: Walthan, MA, USA, 2015; pp. 10–70.

28. Karpenko, M. Investigation of Energy Efficiency of Mobile Machinery Hydraulic Drives. Ph.D. Thesis, Vilnius Gediminas Technical University, Vilnius, Lithuania, 2021. Available online: http://dspace.vgtu.lt/bitstream/1/4269/1/M_Karpenko%20disertacija.pdf (accessed on 5 September 2020).
29. Koo, B. Comparison of finite-volume method and method of characteristics for simulating transient flow in natural-gas pipeline. *J. Nat. Gas Sci. Eng.* **2022**, *98*, 104374. [CrossRef]
30. Praks, P.; Brkić, D. Review of new flow friction equations: Constructing Colebrook's explicit correlations accurately. *Rev. Int. Métodos Numér. Cálc. Diseño Ing.* **2020**, *36*, 41. Available online: https://www.scipedia.com/public/Praks_Brkic_2020a (accessed on 7 November 2022). [CrossRef]
31. Semaškaitė, V.; Bogdevičius, M. Liquefied natural gas regasification technologies. In *Transbaltica XII: Transportation Science and Technology. Transbaltica 2019. Lecture Notes in Intelligent Transportation and Infrastructure*; Prentkovskis, O., Yatskiv (Jackiva), I., Skačkauskas, P., Junevičius, R., Maruschak, P., Eds.; Springer: Cham, Germany, 2022. [CrossRef]
32. Bogdevicius, M.; Suslavicius, V. Hydrodynamic Processes of the Impulse Fire Extinguishing. *Transp. Telecommun.* **2006**, *7*, 342–349.
33. Bajoraityte, I.; Bogdevicius, M. Dynamic processes in the oil pipelines. Part ii. The leak identification by numerical methods. *Transport* **2003**, *18*, 49–55. [CrossRef]
34. Bajoraityte, I.; Bogdevicius, M. Dynamic processes in the main oil pipelines. Part i. Causes of leakage occurrence in oil pipelines and leak identification methods. *Transport* **2002**, *17*, 234–240. [CrossRef]
35. Bogdevicius, M.; Janutiene, J.; Jonikas, K.; Guseinoviene, E.; Draksas, M. Mathematical modeling of oil transportation by pipelines using anti-turbulent additives. *J. Vibroengineering* **2013**, *15*, 419–427.
36. Karpenko, M.; Bogdevicius, M. Investigation of hydrodynamic processes in the system—"axial piston pumps-pipeline-fittings". In *VII International Symposium of Young Researchers Transport Problems 2018*; Silesian University of Technology, Faculty of Transport: Kartowice, Poland, 2018; pp. 832–843.
37. Karpenko, M.; Bogdevicius, M. Investigation into the Hydrodynamic Processes of Fitting Connections for Determining Pressure Losses of Transport Hydraulic Drive. *Transport* **2020**, *35*, 108–120. [CrossRef]
38. Jiang, Y.; Ren, Z.; Yang, X.; Li, Q.; Xu, Y. A steady-state energy flow analysis method for integrated natural gas and power systems based on topology decoupling. *Appl. Energy* **2022**, *305*, 118007. [CrossRef]
39. Garrett, S.J. Chapter 13-introductory numerical methods. In *Introduction to Actuarial and Finanacial Mathematical Methods*; Garrett, S.J., Ed.; Elsevier: Amsterdam, The Netherlands, 2015; pp. 411–463. [CrossRef]
40. Gnedin, N.Y.; Semenov, V.A.; Kravtsov, A.V. Enforcing the Courant–Friedrichs–Lewy condition in explicitly conservative local time stepping schemes. *J. Comput. Phys.* **2018**, *359*, 93–105. [CrossRef]
41. Fedorko, G.; Molnar, V.; Dovicab, M.; Tothb, T.; Fabianova, J. Failure analysis of irreversible changes in the construction of the damaged rubber hoses. *Eng. Fail. Anal.* **2015**, *58*, 31–43. [CrossRef]